Electronic Supplementary Material (ESI) for New Journal of Chemistry.

Electronic Supplementary Information

Synthesis, structure and biological evaluation of mixed ligand oxidovanadium(IV) complexes incorporating 2–(arylazo) phenolates

Sudhir Lima,[a] Atanu Banerjee,[a] Monalisa Mohanty,[a] Gurunath Sahu,[a] Chahat Kausar,[b] Samir Kumar Patra,[b] Eugenio Garribba,[c] Werner Kaminsky,[d] and Rupam Dinda*[,a]

[a]*Department of Chemistry, National Institute of Technology, Rourkela, 769008 Odisha, India. E-mail:* rupamdinda@nitrkl.ac.in

[b]*Department of Life Science, National Institute of Technology, Rourkela 769008, Odisha, India*

[c]*Dipartimento di Chimica e Farmacia, Università di Sassari, Via Vienna 2, I-07100 Sassari, Italy*

[d]*Department of Chemistry, University of Washington, Seattle, Washington 98195, United States*

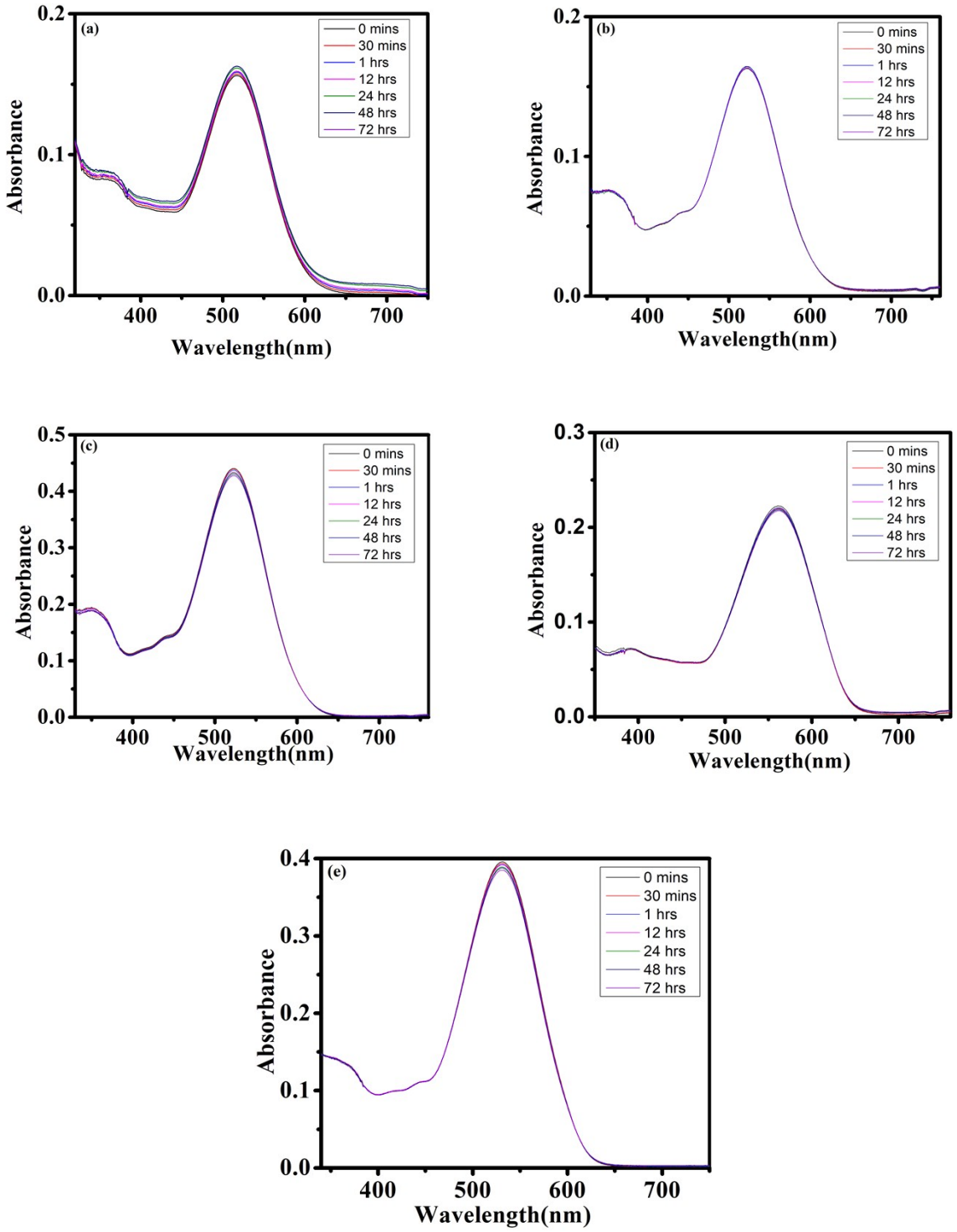

Figure S1. Time dependent UV/vis spectra of compounds (a) $[V^{IV}OL^{1}(bipy)]\cdot H_2O$ (**1**), (b) $[V^{IV}OL^{1}(phen)]$ (**2**), (c) $[V^{IV}OL^{2}(bipy)]$ (**3**), (d) $[V^{IV}OL^{3}(bipy)]$ (**4**) and (e) $[V^{IV}OL^{4}(bipy)]$ (**5**) (2.5×10^{-5} M) in Tris-HCl buffer.

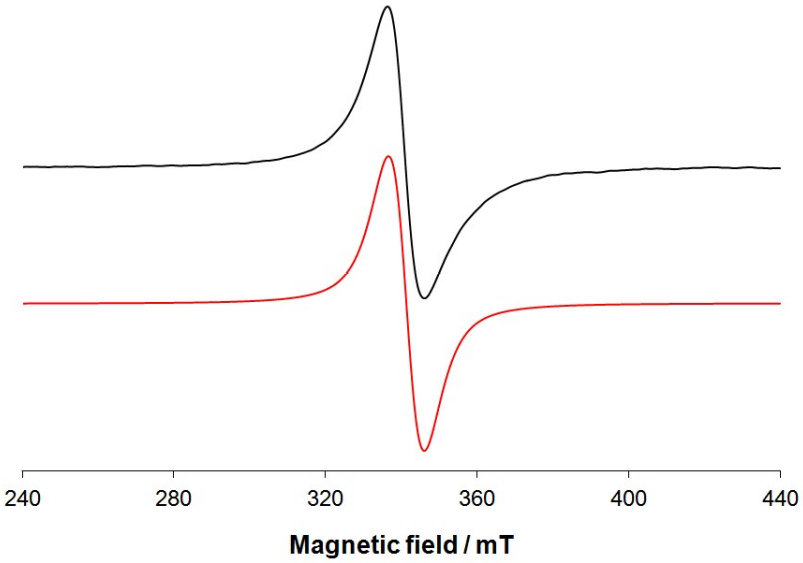

Figure S2. Experimental (in black) and simulated with the software WINEPR SimFonia (in red) isotropic EPR spectrum of complex **5.**

Table S1. Selected bond lengths (Å) and bond angles (degrees) for experimental (Exptl.) and calculated (Calcd.) structures of **1–5**.[a]

	1		**2**		**3**		**4**		**5**	
Bond/angle [b]	Exptl.	Calcd.	Exptl.	Calcd.	Exptl.	Calcd.	Exptl.	Calcd.	Exptl.	Calcd.
V(1)-O(1)	1.969	1.966	1.967	1.964	1.974	1.963	1.985	1.973	1.981	1.965
V(1)-O(2)	1.972	1.953	1.969	1.952	1.963	1.955	1.970	1.955	1.971	1.959
V(1)-O(3)	1.606	1.606	1.607	1.604	1.608	1.606	1.604	1.605	1.606	1.605
V(1)-N(2)	2.056	2.073	2.063	2.071	2.071	2.075	2.053	2.071	2.064	2.072
V(1)-N(3)	2.331	2.311	2.357	2.361	2.338	2.311	2.308	2.307	2.313	2.310
V(1)-N(4)	2.132	2.143	2.136	2.138	2.167	2.143	2.128	2.143	2.137	2.143
O(3)-V(1)-O(1)	99.3	100.0	100.9	100.2	98.8	100.1	97.0	99.5	97.5	100.0
O(3)-V(1)-O(2)	101.3	105.1	102.1	104.9	104.1	104.9	103.5	105.2	104.2	105.0
O(3)-V(1)-N(2)	105.1	104.4	104.6	105.0	101.9	104.6	105.3	103.9	104.1	104.1
O(3)-V(1)-N(3)	168.2	161.7	178.0	163.3	163.4	161.8	165.3	161.6	165.1	161.7
O(3)-V(1)-N(4)	95.6	90.3	94.8	90.8	93.3	90.3	95.4	90.1	95.4	90.2
O(1)-V(1)-O(2)	157.1	153.0	155.4	153.1	154.7	153.0	157.3	153.0	156.2	152.9
N(2)-V(1)-N(4)	159.1	164.6	160.6	163.8	160.8	164.4	157.1	165.0	158.1	164.8

[a] Distances in Å and angles in degrees. [b] For the numbers of atoms, see Figure 3 of the main text.

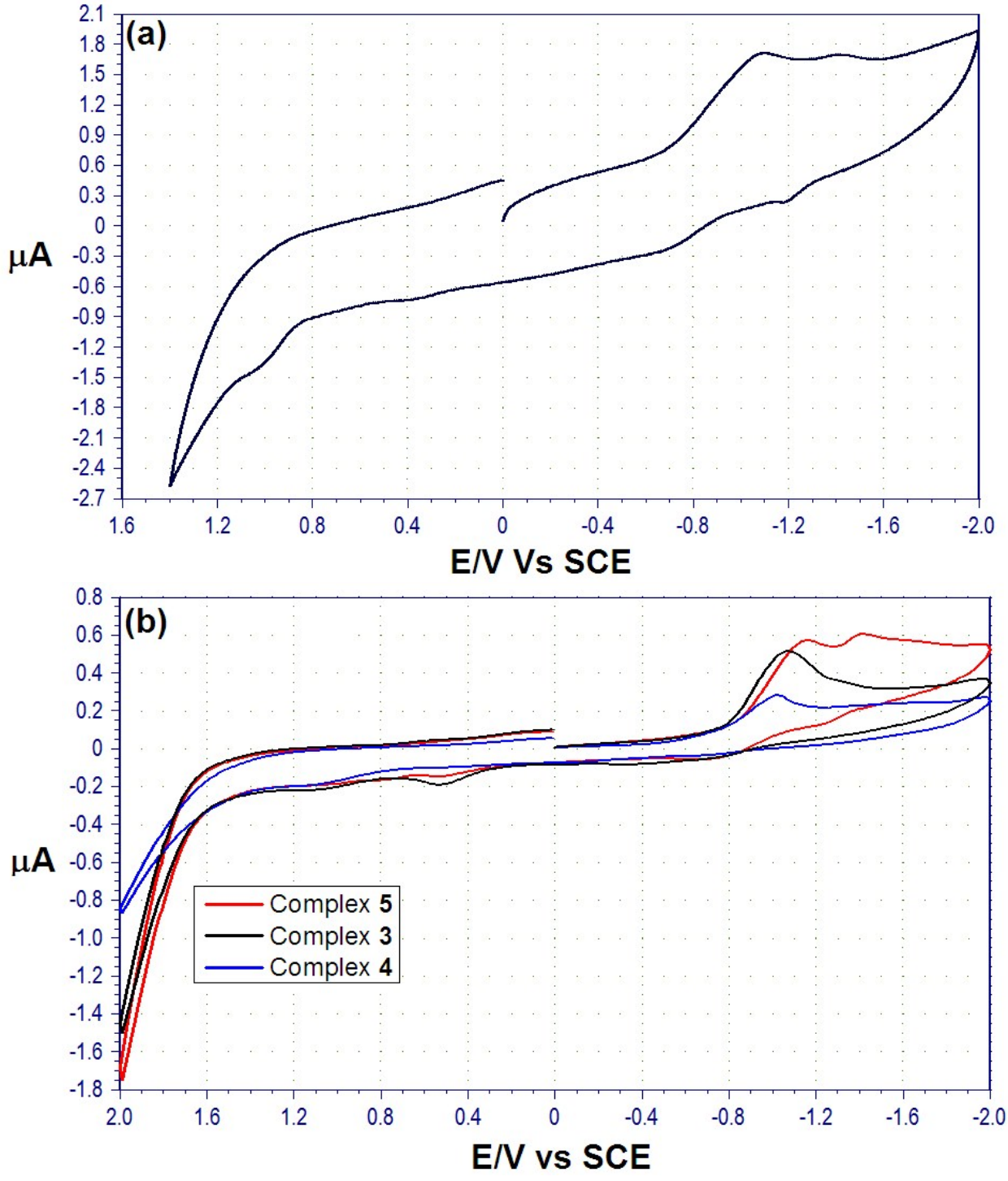

Figure S3. (a) Depicts the cyclic voltammogram of complex [$V^{IV}OL^{1}$(phen)] (**2**) and (b) depicts the voltammogram of complexes [$V^{IV}OL^{2}$(bipy)] (**3**), [$V^{IV}OL^{3}$(bipy)] (**4**) and [$V^{IV}OL^{4}$(bipy)] (**5**) in acetonitrile at a scan rate of 100 mV s^{-1}

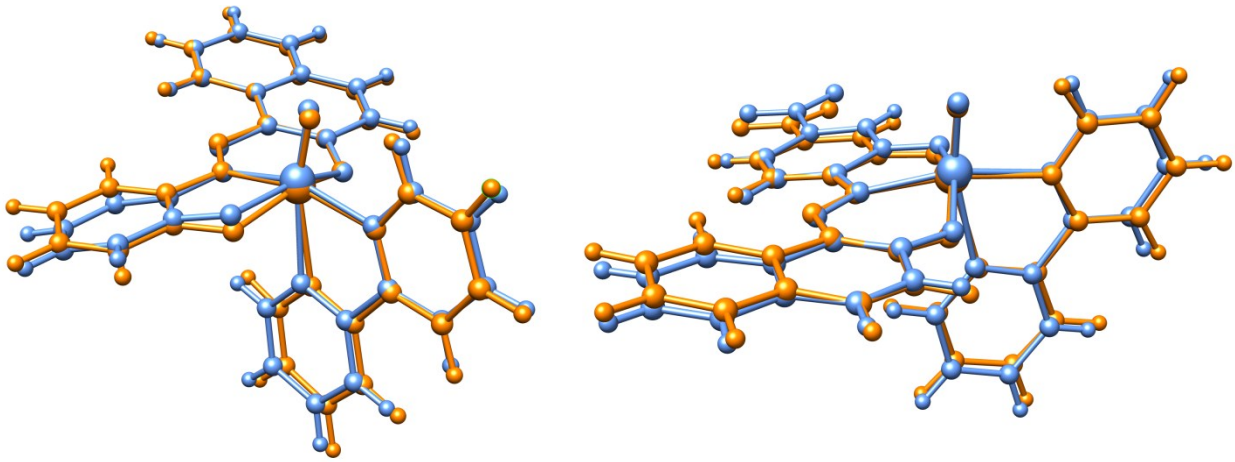

Figure S4. Overlap of the XRD (in blue) and DFT optimized (in orange) structures of the complexes **1** (left) and **4** (right).

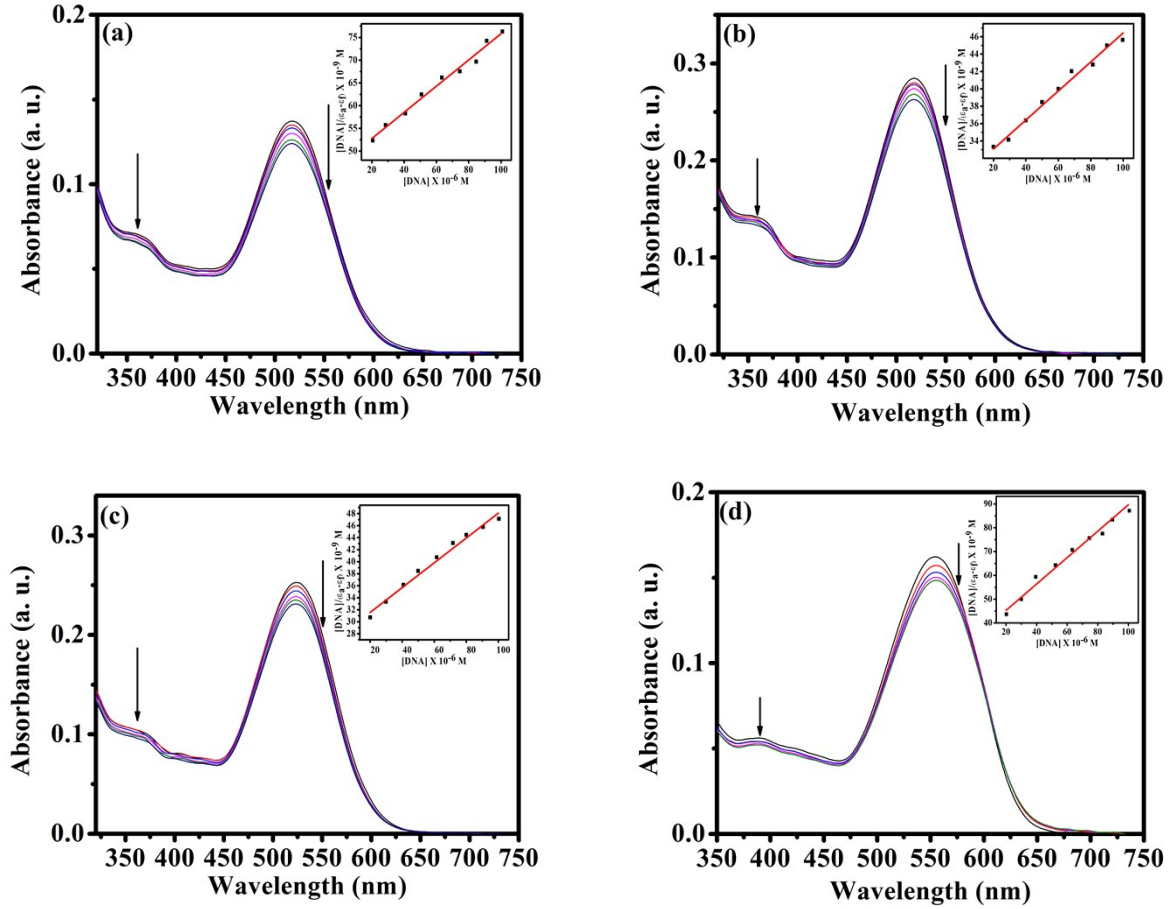

Figure S5. Absorption spectroscopic study of complexes **1** (a), **3** (b), **4** (c) and **5** (d) (25 μM) with increasing concentrations of CT–DNA (0–100 μM) in 50 mM Tris-HCl buffer (pH 8.0). Arrow shows the changes in absorbance with respect to an increase in the CT-DNA concentration. The inset shows the linear fit of [DNA]/($\varepsilon_a - \varepsilon_f$) vs [DNA].

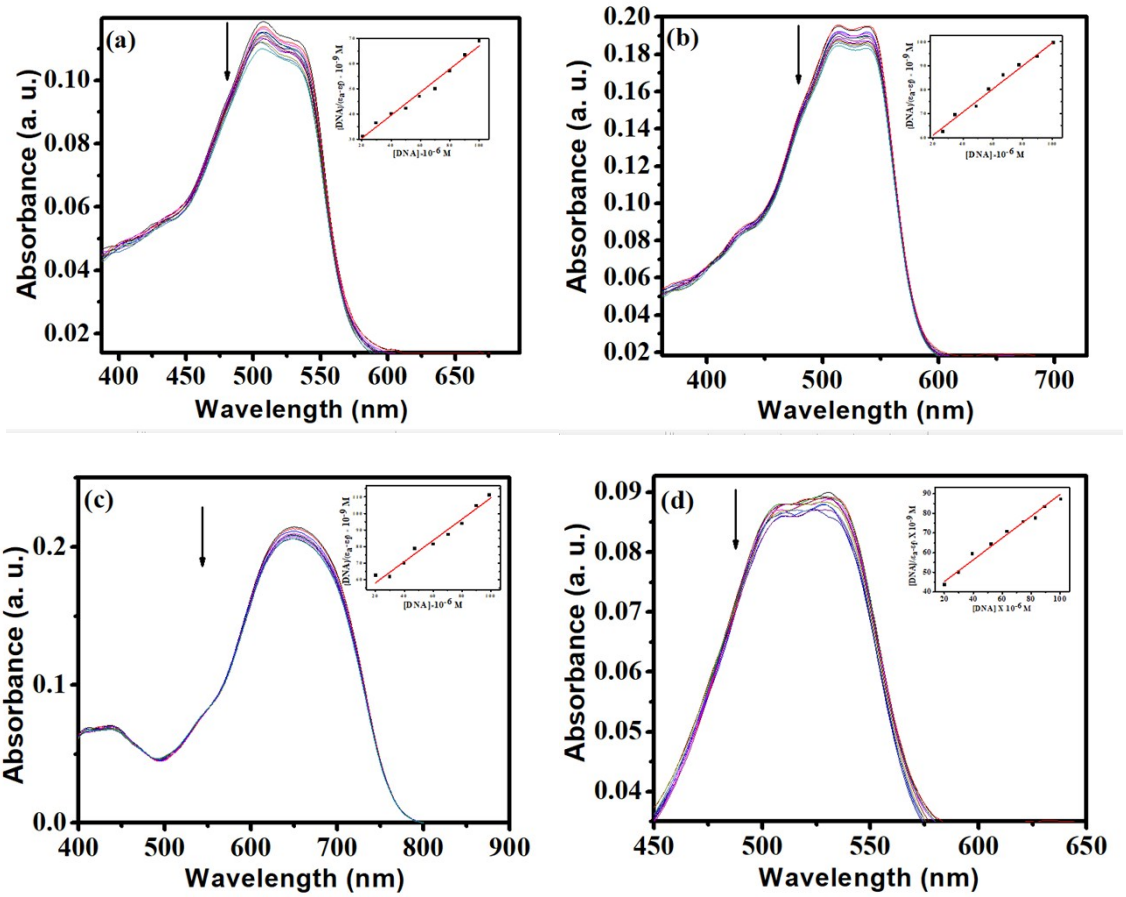

Figure S6. Absorption spectroscopic study of ligands H_2L^1 (a), H_2L^2 (b), H_2L^3 (c) and H_2L^4 (d) with increasing concentrations of CT–DNA (0–100 µM) in 50 mM Tris–HCl buffer (pH 8.0). Arrow shows the changes in absorbance with respect to an increase in the CT–DNA concentration. The inset shows the linear fit of $[DNA]/(\varepsilon_a - \varepsilon_f)$ vs [DNA].

Table S2. DNA binding parameters of ligands H_2L^{1-4}.

Complexes	Binding constant (K_b)[a] (M^{-1})
H_2L^1	9.81×10^3
H_2L^2	2.98×10^2
H_2L^3	1.13×10^3
H_2L^4	1.43×10^2

[a] DNA binding constants were determined by the UV-vis spectral method.

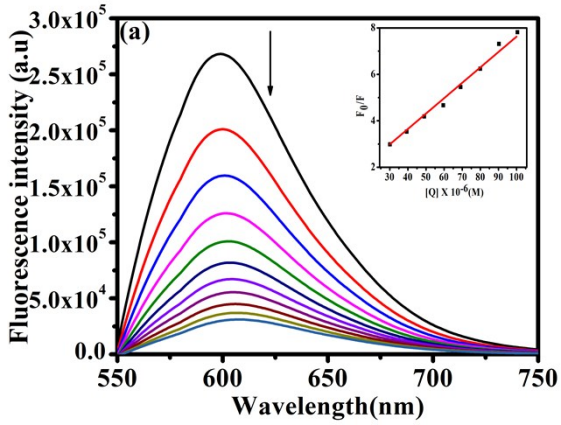
(a)
Fluorescence intensity (a.u)
Wavelength(nm)
F_0/F
[Q] X 10^{-6}(M)

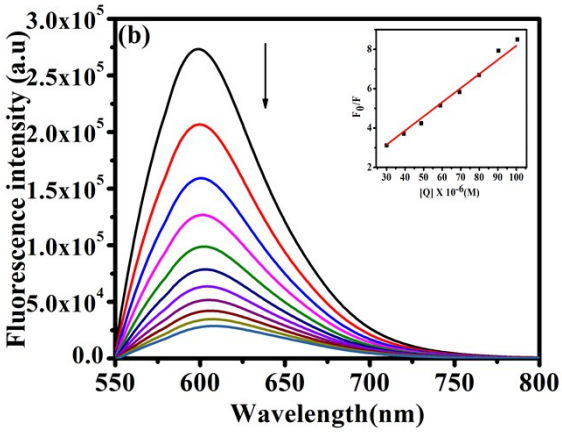
(b)
Fluorescence intensity (a.u)
Wavelength(nm)
F_0/F
[Q] X 10^{-6}(M)

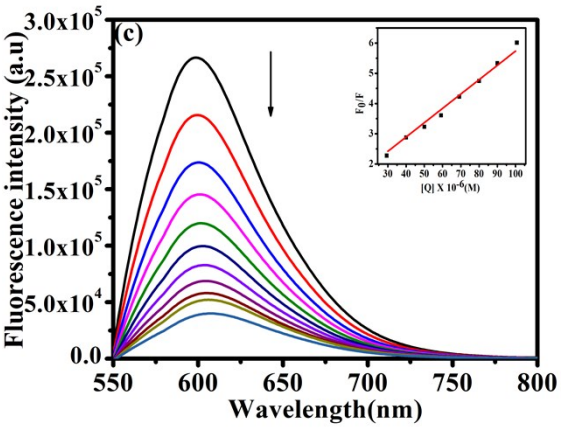
(c)
Fluorescence intensity (a.u)
Wavelength(nm)
F_0/F
[Q] X 10^{-6}(M)

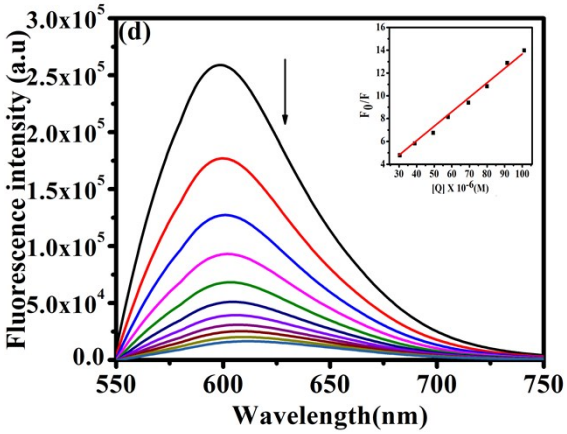
(d)
Fluorescence intensity (a.u)
Wavelength(nm)
F_0/F
[Q] X 10^{-6}(M)

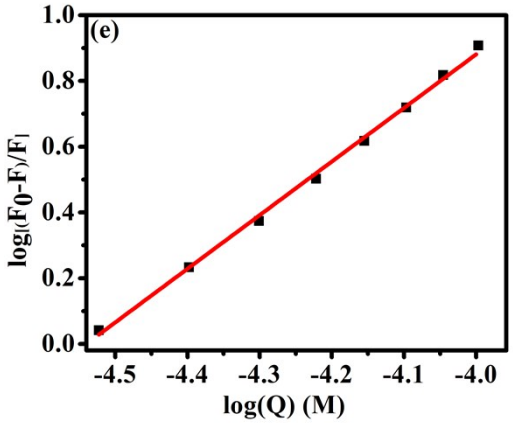
(e)
$\log((F_0-F)/F)$
log(Q) (M)

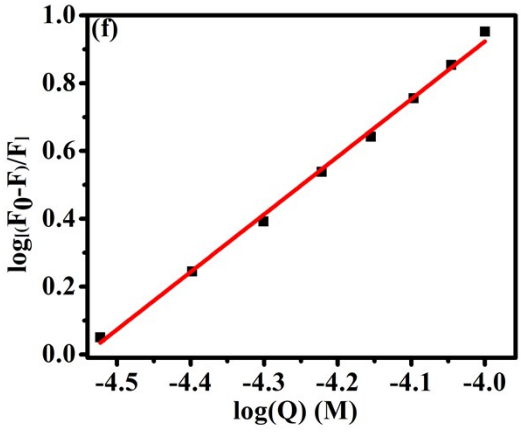
(f)
$\log((F_0-F)/F)$
log(Q) (M)

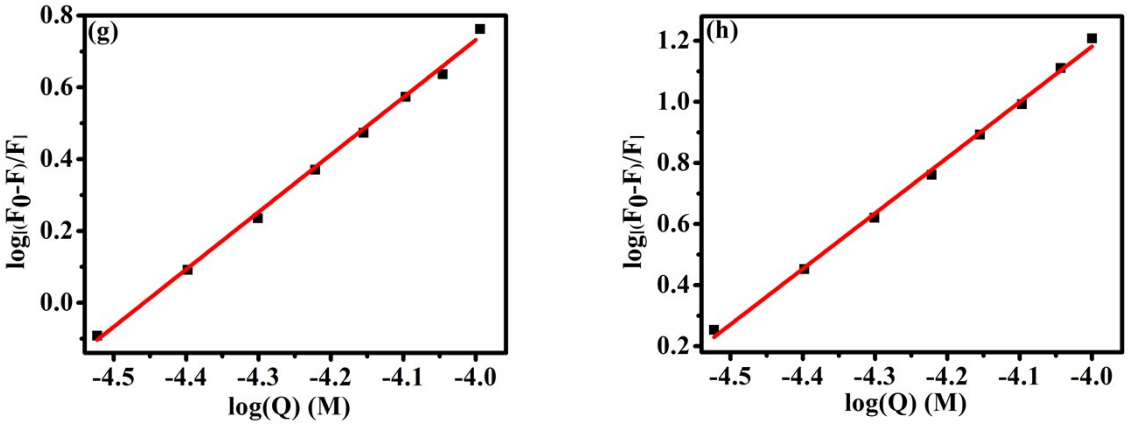

Figure S7. Fluorescence quenching of EB (10 μM) by complexes **1** (a), **2** (b), **3** (c) and **5** (d) (0–100 μM each) and the inset shows the Stern-Volmer plot of complexes **1** (a), **2** (b), **3** (c) and **5** (d); The Scatchard plot has been mentioned as complexes **1** (e), **2** (f), **3** (g) and **5** (h).

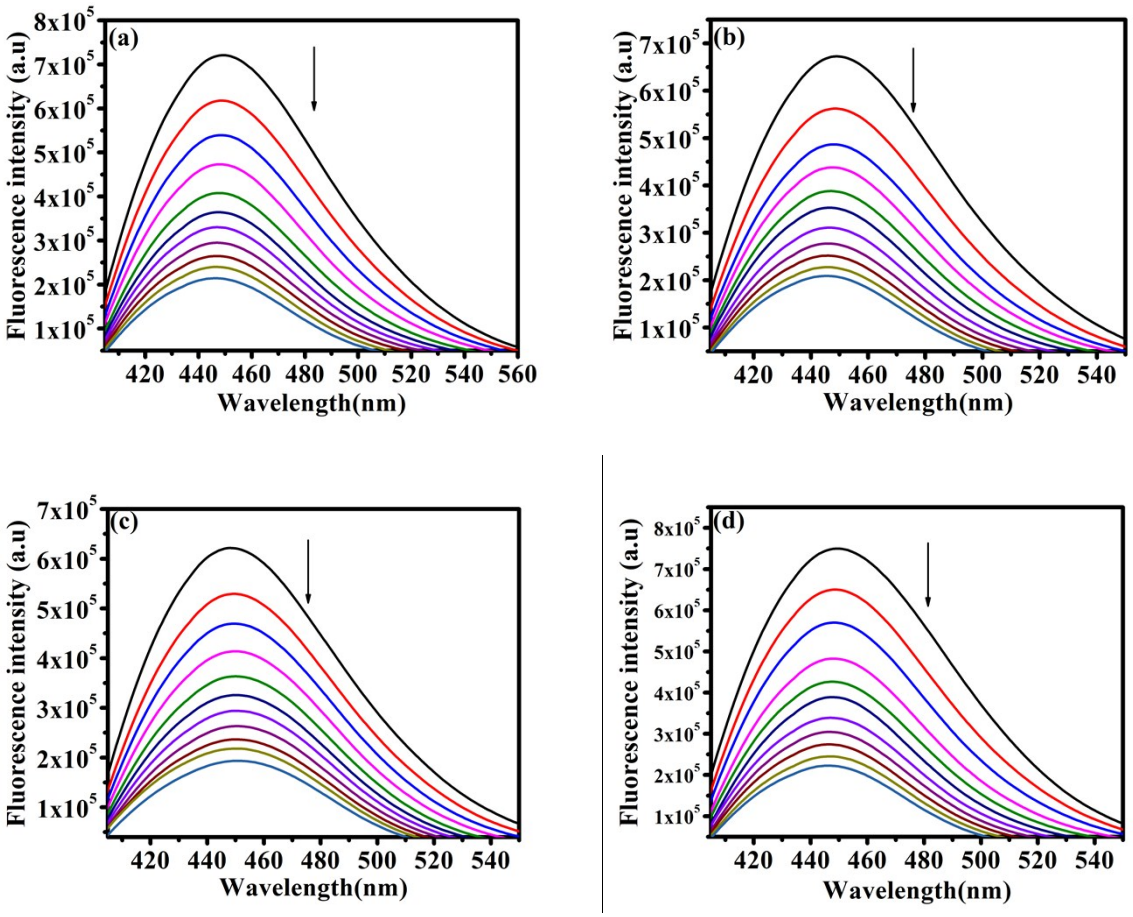

Figure S8. Fluorescence quenching of DAPI (10 µM) by complexes **2** (a), **3**(b), **4**(c) and **5** (d) (0–100 µM each).

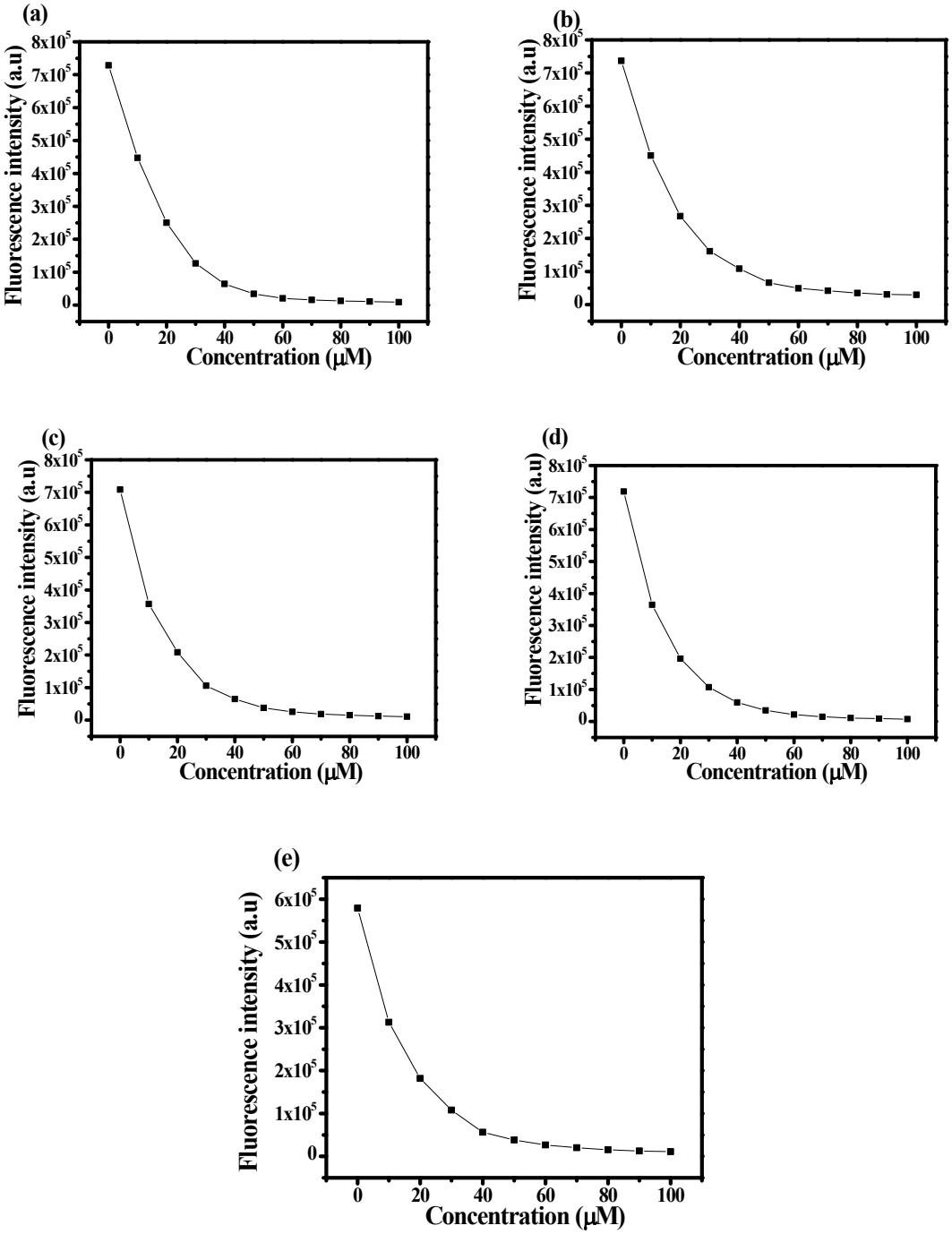

Figure S9. Fluorescence quenching of BSA (10 μM) by complexes **1** (a), **2** (b), **3** (c), **4** (d) and **5** (e) (0–100 μM each).

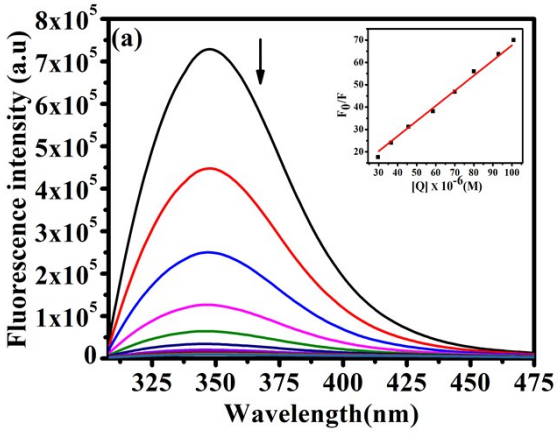
(a)
Fluorescence intensity (a.u)
Wavelength(nm)
F0/F
[Q] X 10-6(M)

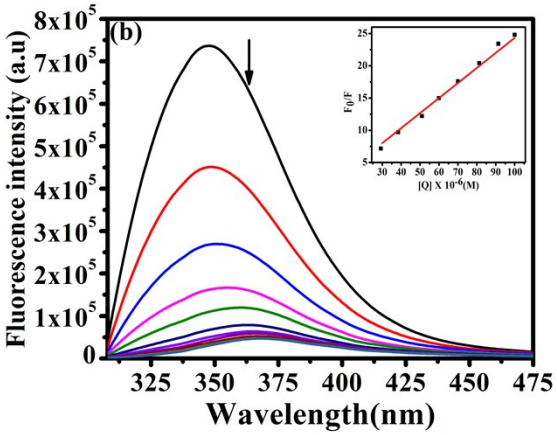
(b)
Fluorescence intensity (a.u)
Wavelength(nm)
F0/F
[Q] X 10-6(M)

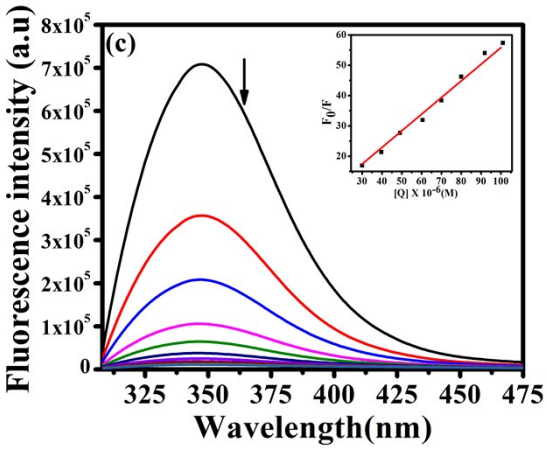
(c)
Fluorescence intensity (a.u)
Wavelength(nm)
F0/F
[Q] X 10-6(M)

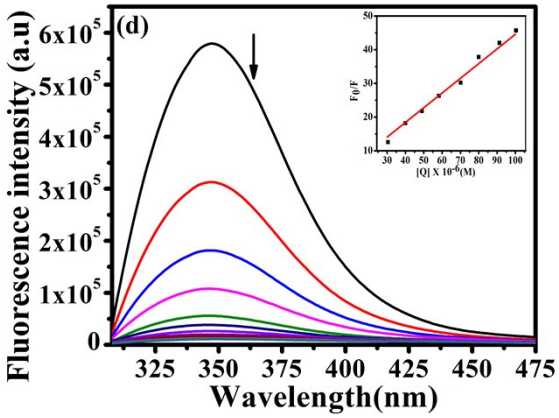
(d)
Fluorescence intensity (a.u)
Wavelength(nm)
F0/F
[Q] X 10-6(M)

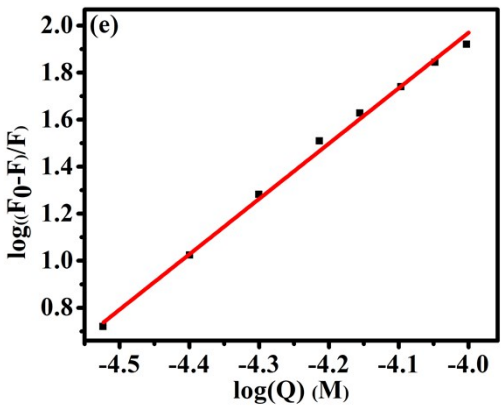
(e)
log((F0-F)/F)
log(Q) (M)

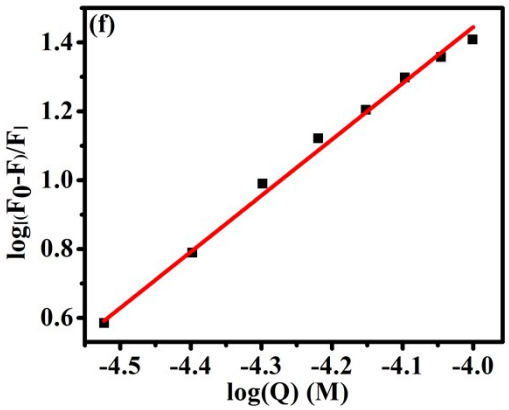
(f)
log((F0-F)/F)
log(Q) (M)

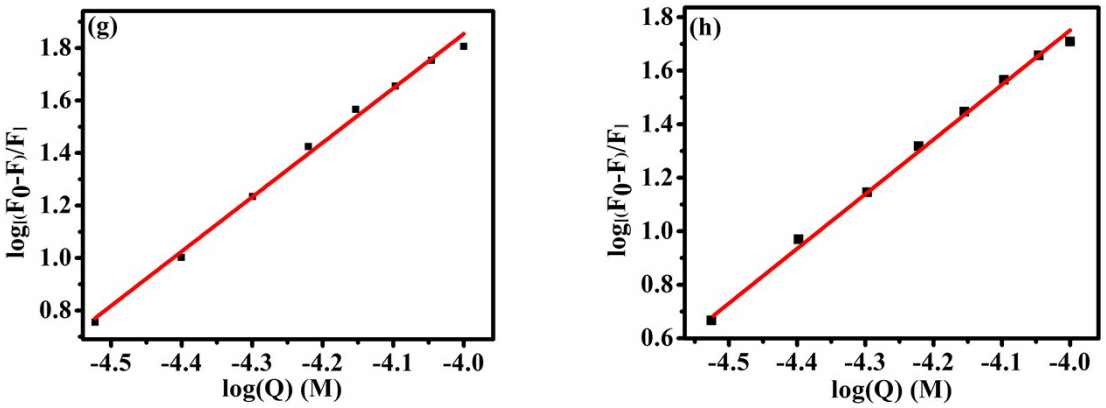

Figure S10. Fluorescence quenching of BSA (10 µM) by complexes **1** (a), **2** (b), **3** (c) and **5** (d) (0–100 µM each) and the inset shows the Stern–Volmer plot of complexes **1** (a), **2** (b), **3** (c) and **5** (d); The Scatchard plot has been mentioned as complexes **1** (e), **2** (f), **3** (g) and **5** (h).

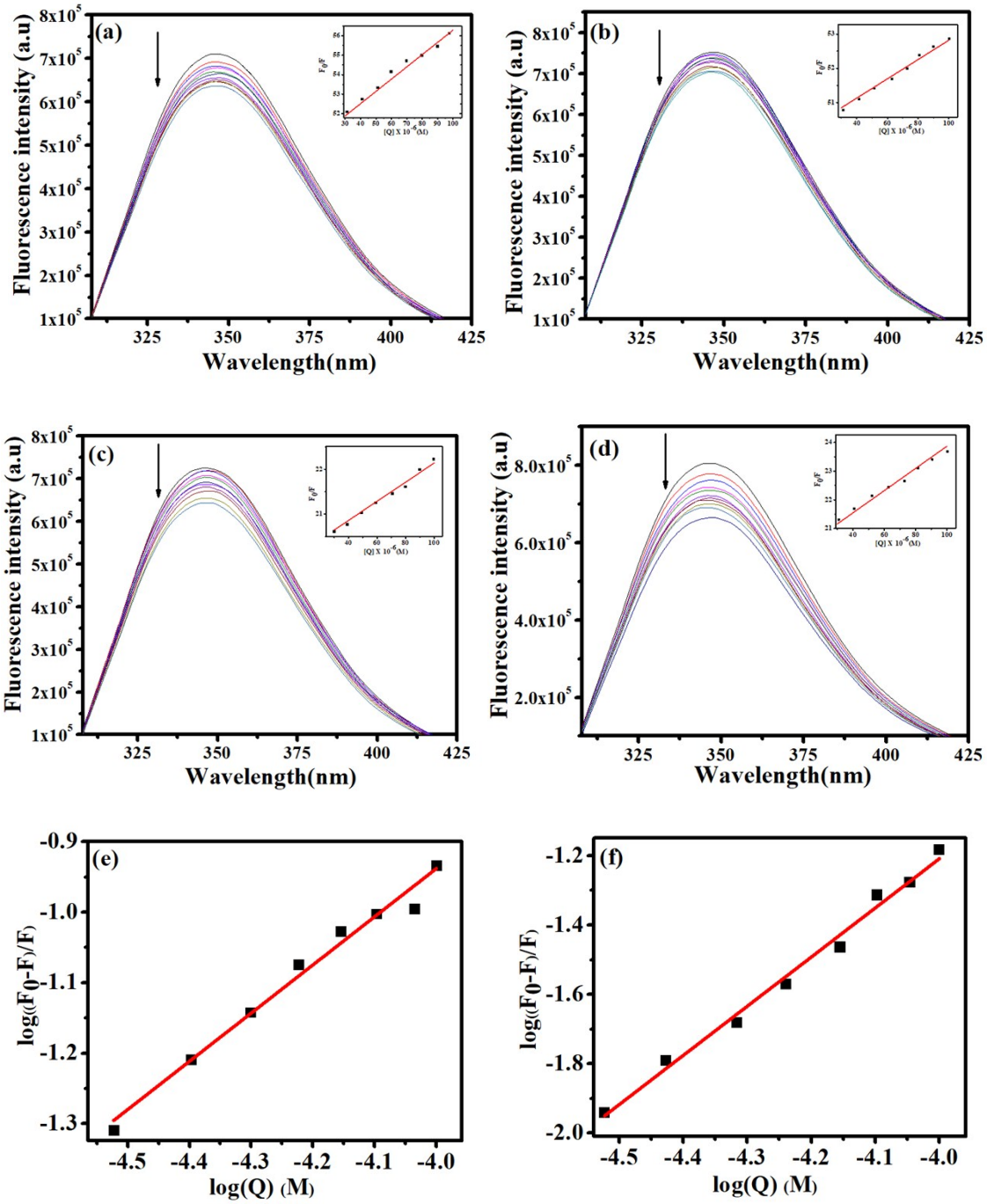
(a)
(b)
(c)
(d)
(e)
(f)
Fluorescence intensity (a.u)
Wavelength(nm)
log((F0-F)/F)
log(Q) (M)
F0/F
[Q] X 10-6 (M)

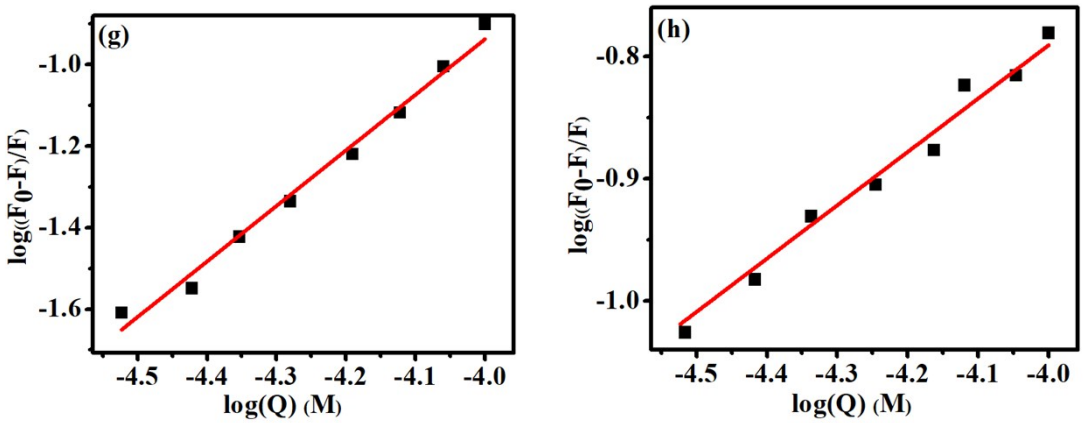

Figure S11. Fluorescence quenching of BSA (10 µM) by ligands H_2L^1 (a), H_2L^2 (b), H_2L^3 (c) and H_2L^4 (d) (0–100 µM each) and the inset shows the Stern–Volmer plot of ligands H_2L^1 (a), H_2L^2 (b), H_2L^3 (c) and H_2L^4 (d); The Scatchard plot has been mentioned as ligands H_2L^1 (e), H_2L^2 (f), H_2L^3 (g) and H_2L^4 (h).

Table S3. BSA binding parameters of the ligands ($H_2L^{1–4}$).

Ligand	Stern–Volmer Constant K_{sv} (M^{-1})	Bimolecular rate constant K_q($M^{-1}s^{-1}$)	Binding Constant K_a (M^{-1})	Number of binding sites (n)
H_2L^1	1.2×10^3	1.9×10^{11}	6.3×10^1	0.68
H_2L^2	5.6×10^2	9.1×10^{10}	3.2×10^4	1.40
H_2L^3	1.1×10^3	1.7×10^{11}	3.2×10^4	1.36
H_2L^4	1.9×10^3	3.1×10^{11}	1.0×10^1	0.43

1. Cytotoxicity study on non-cancerous human epidermal keratinocyte cell line HaCaT

Methods

Cytotoxicity of the complexes (**1**–**5**) was evaluated against A549 (lung cancer) cell line by MTT assay. In order to check the cytotoxic effect on cell viability of physiological cells, we have performed similar studies on non-cancerous human epidermal keratinocyte cell line HaCaT. HaCaT cells were cultured in DMEM media and the subsequent experiment was performed as per the protocol mentioned in the *Experimental Section* (for A549 cell line), using four different concentrations (100, 50, 25 and 12.5 µg/ml) of the complexes prepared in complete DMEM media. Cytotoxicity of the compound was analyzed by measuring the % cell viability of the cells.

Results

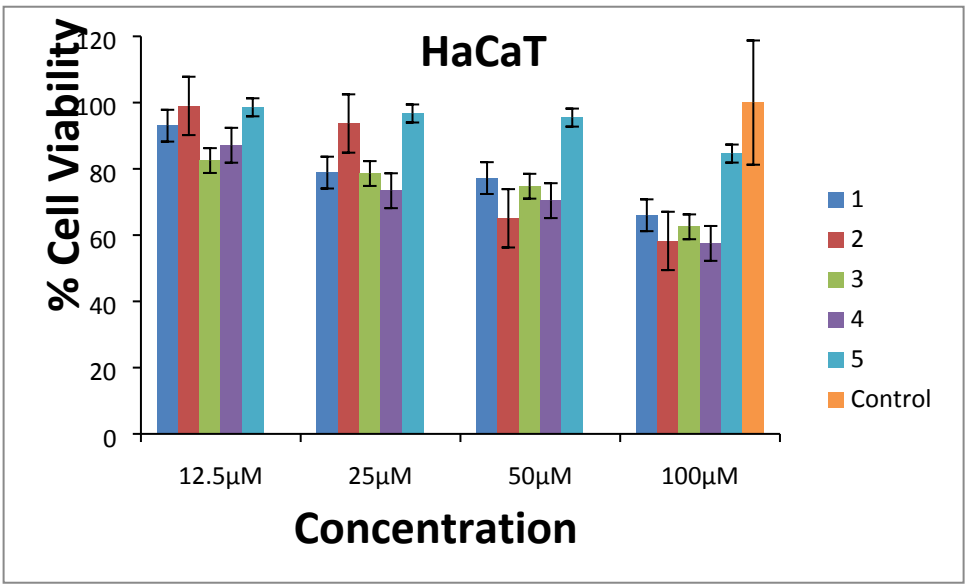

Fig. S12. Effect of **1**–**5** on cell viability of HaCaT. The cells were treated with different concentrations of the test compounds for 48 h and then cell viability was calculated by MTT assay.

Table S4. Comparative study of IC_{50} value of the compounds against A549 and HaCaT.

Complexes	IC_{50} (µM)	IC_{50} (µM)
	A549	HaCaT
1	49.66 ± 0.11	144± 0.02
2	44.72 ± 0.04	211± 0.04
3	53.80 ± 0.07	568± 0.07
4	48.92 ± 0.30	380± 0.04
5	57.54 ± 0.28	614± 0.24

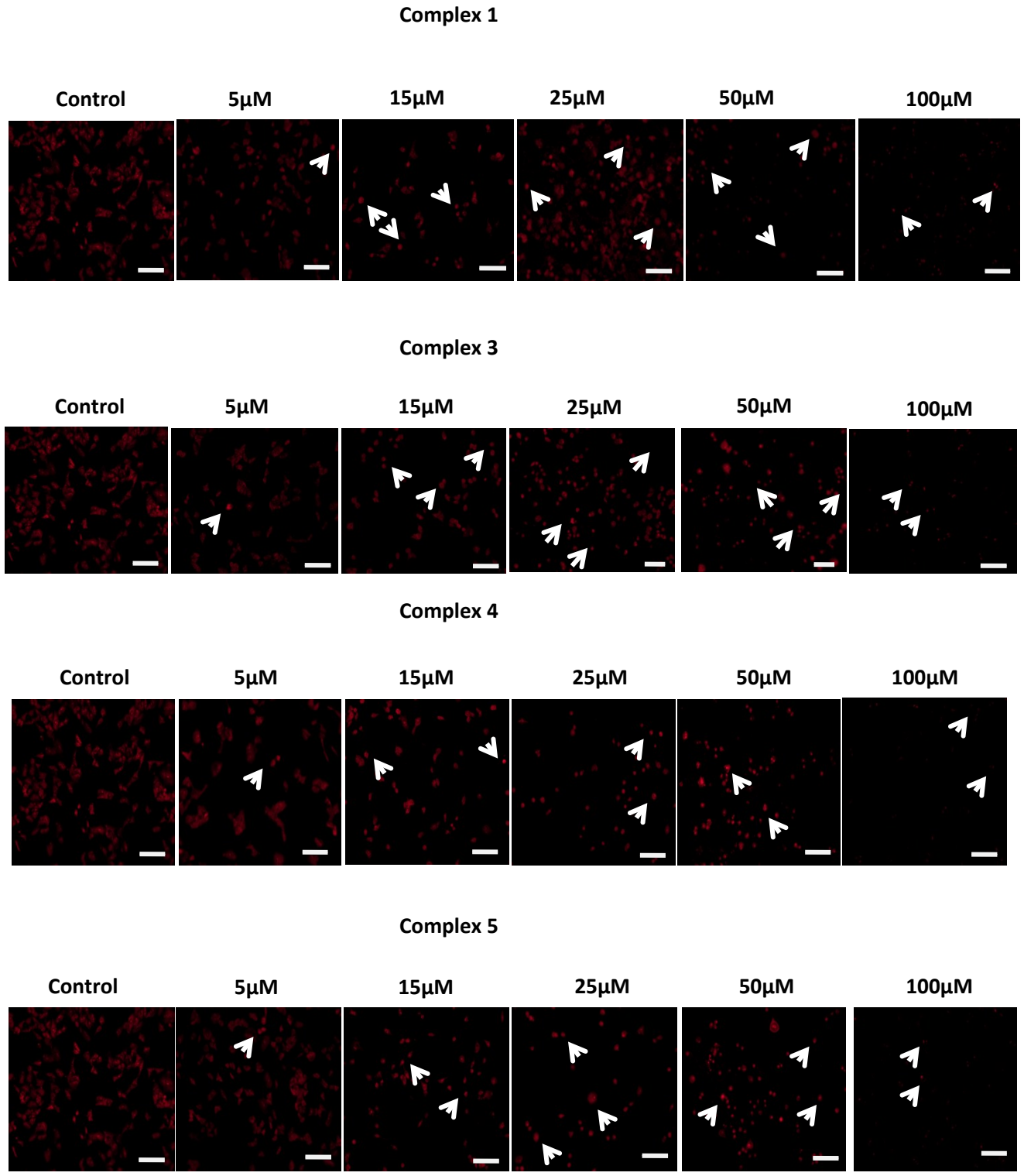

Figure S13. PI staining of complexes of A549 (Lung cancer line) taken in Olympus IX 74 fluorescence microscope. Arrows showing the morphological changes in nuclei of A549 cells observed on applying increasing concentrations (5, 15, 25, 50 and 100 µM) of complexes **1**, **3**, **4** and **5** at different concentrations in comparison to control. The scale bar corresponds to 100 µm.

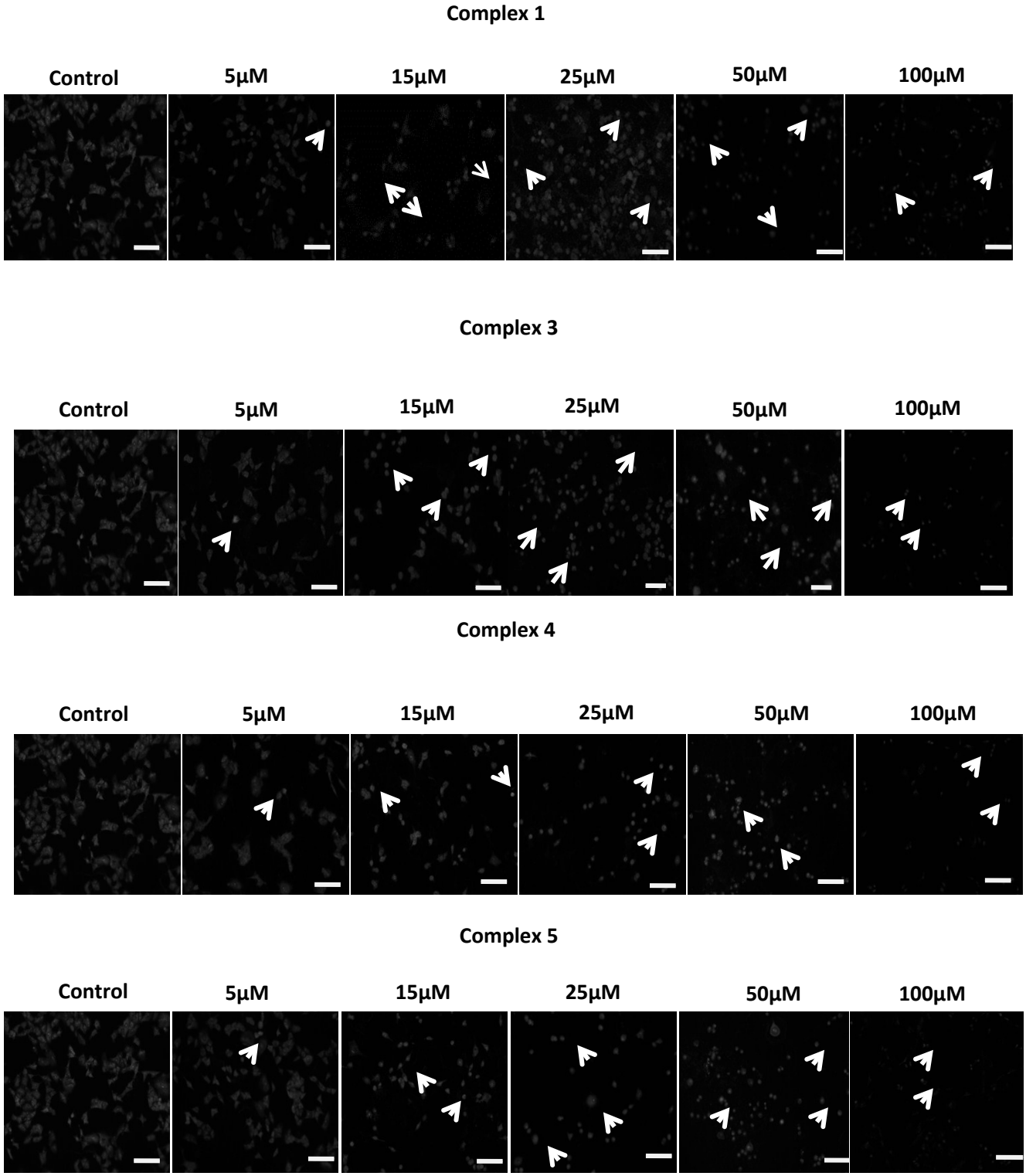

Figure S14. PI staining of complexes of A549 (Lung cancer line) taken in Olympus IX 74 fluorescence microscope. Arrows showing the morphological changes in nuclei of A549 cells observed on applying increasing concentrations (5, 15, 25, 50 and 100 µM) of complexes **1**, **3**, **4** and **5** at different concentrations in comparison to control. The scale bar corresponds to 100 µm.